

Polarization aberrations caused by differential transmission and phase shift in high-numerical-aperture lenses: theory, measurement, and rectification

Michael Shribak, MEMBER SPIE

Shinya Inoué

Rudolf Oldenbourg, MEMBER SPIE

Marine Biological Laboratory

Woods Hole, Massachusetts 02543

E-mail: mshribak@mbl.edu

Abstract. We present a theoretical and experimental study of radially symmetric aberration caused by the differential transmission and phase shift of p - and s -polarized components of an axial beam passing through spherical lenses and plane parallel plates. We give a general description of the aberrations for an axial beam. The extinction is calculated as a function of the numerical aperture for uncoated lenses and for plane parallel plates. In our theoretical analysis, the polarization of output rays is described as a function of the input ray parameters, the shape factor, and refractive index of the lenses used. For rays that are inclined to the optical axis, optimal lens shape factors that minimize the rays' polarization aberrations are found. Techniques for measurement of radially symmetric birefringence in a lens system are described. Finally, we discuss strategies for polarization rectification and introduce new designs including meniscus rectifiers and a liquid crystal rectifier that can actively compensate a wide variety of polarization aberrations. Good correlations between theory and experimental results for microscope optical systems with coated and uncoated optical elements are found. Our results enable us to suppress depolarization and remove anomalous diffraction in a modern microscope equipped with high-numerical-aperture lenses. © 2002 Society of Photo-Optical Instrumentation Engineers. [DOI: 10.1117/1.1467669]

Subject terms: polarization; microscopy; aberration; rectifier; compensator; birefringence; diattenuation.

Paper PL-010 received Sep. 7, 2001; revised manuscript received Dec. 13, 2001; accepted for publication Dec. 31, 2001.

1 Introduction

The extinction factor of a wide-field polarizing microscope rapidly drops as the numerical aperture of the objective and condenser lens is raised, even with a high-quality polarizing system and the use of carefully selected lenses that are free from strain birefringence and birefringent inclusions.¹⁻³ The loss of extinction originates from the differential transmission (diattenuation) and phase shift (retardance) between the p - and s -polarization components of rays that pass through steep optical interfaces. Differential transmission and phase shift lead to spatial polarization changes in the exit pupil plane called "polarization aberrations."⁴ The polarization aberrations cause undesirable polarization components (depolarization⁵) that reduce the extinction in the image plane. The polarization aberrations result in four bright quadrants separated by a dark cross, known as the Maltese cross, that is seen conoscopically in the exit pupil of a high-numerical-aperture (NA) strain-free lens system between crossed linear polarizers in the absence of a specimen. If crossed circular polarizers are used instead, a dark central disk is surrounded by a bright ring in the exit pupil. Polarization aberrations can also give rise to anomalous diffraction, caused by a four-leaf clover pattern that replaces the Airy disk when imaging weakly birefringent objects between crossed linear polarizers.^{6,7} In

general, polarization aberrations modify the point spread function and the optical transfer function of optical systems.⁸ Various possible theoretical pictures of polarization state distributions in the exit pupil of lens systems based on a paraxial approximation of the effect of polarization aberrations can be found in published papers.^{4,9} Other polarization optical devices, where lenses are used between polarizers, such as ellipsometers, polarimetric sensors, and optical disk systems with polarization reading of information,¹⁰⁻¹² must also take into account the depolarization caused by the factors considered here. In a single-point scanning confocal imaging system, however, polarization aberrations that occur in different quadrants of the exit pupil cancel each other and the extinction remains high even when high-NA lenses are used.¹³

2 General Description of Polarization Aberrations of an Axial Beam Passing Through Lens Surfaces

An axial beam can be considered as being composed of individual rays that travel through lens surfaces each under a different plane and angle of incidence. Because of the rotational symmetry of a lens the differential amplitude transmission and phase shift between the p - and s -polarization components of rays are radially symmetric.

Let us consider an axial beam in a lens optical system. We choose polar coordinates at the center of an entrance pupil that has unit radius. The polarization change of a ray with the radial coordinate ρ ($0 \leq \rho \leq 1$) and azimuth θ ($0 \leq \theta \leq 2\pi$) is determined by the Jones matrix $\mathbf{M}(\rho, \theta)$:

$$\begin{aligned} \mathbf{M}(\rho, \theta) &= \begin{pmatrix} \cos \theta & -\sin \theta \\ \sin \theta & \cos \theta \end{pmatrix} \cdot \begin{pmatrix} T_p(\rho) \exp[i\Delta_p(\rho)] & 0 \\ 0 & T_s(\rho) \exp[i\Delta_s(\rho)] \end{pmatrix} \cdot \begin{pmatrix} \cos \theta & \sin \theta \\ -\sin \theta & \cos \theta \end{pmatrix} \\ &= \frac{1}{2} T_s e^{i\Delta_s} \begin{pmatrix} \mu e^{i\Delta} + 1 + (\mu e^{i\Delta} - 1) \cos 2\theta & (\mu e^{i\Delta} - 1) \sin 2\theta \\ (\mu e^{i\Delta} - 1) \sin 2\theta & \mu e^{i\Delta} + 1 - (\mu e^{i\Delta} - 1) \cos 2\theta \end{pmatrix}. \end{aligned} \quad (1)$$

Here T_p and T_s are amplitude transmission coefficients of the p - and s -polarization components, and Δ_s and Δ_p are phases of the components after traversing the optical system. Parameters μ and Δ describe the differential transmission and radial retardance, respectively, where $\mu = T_p/T_s$ and $\Delta = \Delta_p - \Delta_s$. A small angle ξ is also used for the description of the differential transmission $\xi = \tan^{-1}(\mu - 1/\mu + 1) \approx (1/2)(\mu - 1)$. Typically, in the center of the pupil when $\rho = 0$, there is no differential transmission or phase shift, and the parameter μ equals 1 and the turn angle ξ is 0 deg. Toward the periphery of the pupil when ρ increases, the values of parameters μ and ξ also increase. Differential transmission is usually stronger in a microscope with dry, high-NA condenser and objective lenses when compared to oil-immersion systems. Radial retardance originates from the oblique passage of a ray through optical multilayer coatings and from radially symmetric stress in lenses.

If the optical system, including the slide and cover slip that lie between the condenser and objective lenses, has N surfaces, then

$$T_p = \prod_{k=1}^N t_{pk}, \quad T_s = \prod_{k=1}^N t_{sk}, \quad \mu = \prod_{k=1}^N \hat{\mu}_k, \quad (2)$$

$$\xi \approx \sum_{k=1}^N \hat{\xi}_k, \quad \Delta = \sum_{k=1}^N \delta_k,$$

where t_{pk} and t_{sk} are the amplitude transmission coefficients, and δ_k is the phase shift for the optical surface with number k . Hence, $\hat{\mu}_k = t_{pk}/t_{sk}$ and $\hat{\xi}_k = (1/2)(\hat{\mu}_k - 1)$.

Eigenvectors of the matrix of Eq. (1) are linearly polarized. The polarization direction of the p component is along the azimuth angle θ of the rays. Coefficients of the differential transmission and radial retardance only depend on the radius ρ . The differential transmission and phase shift lead to a polarization component in the beam that is orthogonal to its initial polarization.

The orthogonal polarization component reduces the extinction of an optical system. The intensity ratio of the initial polarization I'_x over the orthogonal polarization I'_y of the output beam is called the system extinction factor κ of the complete optical system, such as a microscope. This extinction is measured in the image plane. The extinction factor of the complete system can be derived from the ex-

tingtion of each individual ray $\eta(\rho, \theta) = [E'_x(E'_x)^*]/[E'_y(E'_y)^*]$, which can be measured in the exit pupil plane:

$$\begin{aligned} \kappa &= \frac{I'_x}{I'_y} = \frac{\int_0^{2\pi} \int_0^1 I(\rho, \theta) (1 - \eta^{-1}) \rho d\rho d\theta}{\int_0^{2\pi} \int_0^1 I(\rho, \theta) \eta^{-1} \rho d\rho d\theta} \\ &\approx \frac{\int_0^{2\pi} \int_0^1 I(\rho, \theta) \rho d\rho d\theta}{\int_0^{2\pi} \int_0^1 I(\rho, \theta) (\rho/\eta) d\rho d\theta}, \end{aligned} \quad (3)$$

where $I(\rho, \theta)$ is the intensity distribution of the initial beam in the entrance pupil, and E'_x and E'_y are amplitudes of orthogonal polarization components of the ray after the optical system. Note that there are also other sources of depolarization in optical systems such as the scattering of light by dust, contaminations, and mountings, and the birefringence of glass. These should be removed carefully.

In the strict sense the preceding analysis treats only "on-axis" beams. However, we are here concerned with high-NA microscope systems with large magnification that image only a small field of view. All rays that pass through this small field of view can be considered "on-axis" beams. For example, the objective CFN DIC Plan Achromat 40 \times with NA=0.7 (Nikon, part 85031) has a focal length of 4 mm and a field of view radius of 0.06 mm, approximately. In this case, the difference angle between a ray from a peripheral point in the object and a ray from its center, which cross in the same pupil point, is less than 0.9 deg in the pupil center and less than 0.6 deg for the pupil periphery. Hence, peripheral object points will show almost the same extinction as the central point and our results are expected to apply for the entire field of view of a high-NA microscope.

Let us consider several particular cases. When the initial beam is linearly polarized $\mathbf{E} = \begin{pmatrix} 1 \\ 0 \end{pmatrix}$ then the field amplitude of the output rays can be written as

$$\mathbf{E}' = \frac{1}{2} T_s e^{i\Delta_s} \begin{bmatrix} \mu e^{i\Delta} + 1 + (\mu e^{i\Delta} - 1) \cos 2\theta \\ (\mu e^{i\Delta} - 1) \sin 2\theta \end{bmatrix}. \quad (4)$$

This equation is derived by multiplication of the matrix of Eq. (1) and the vector \mathbf{E} . The extinction η of a ray is determined by

$$\eta = \frac{(\mu+1)^2 + (\mu-1)^2 \cos^2 2\theta - 4\mu \sin^2(\Delta/2) \sin^2 2\theta}{[(\mu-1)^2 + 4\mu \sin^2(\Delta/2)] \sin^2 2\theta}$$

$$\approx \frac{1}{[\tan^2 \xi + \sin^2(\Delta/2)] \sin^2 2\theta}. \quad (5)$$

In the last term, the parameter ξ is used instead of parameter μ . That enables us to simplify the formula and its analysis.

As follows from Eq. (5), when the optical system is put between two crossed linear polarizers, the image of the exit pupil has a cross shape. The cross branches are parallel to the polarizers.

If there is differential transmittance only but no retardance, then

$$\mathbf{E}' = \frac{T_p + T_s}{2} \begin{pmatrix} 1 + \tan \xi \cos 2\theta \\ \tan \xi \sin 2\theta \end{pmatrix}. \quad (6)$$

Thus all output rays will be linearly polarized with a small rotation of the polarization plane α compared to the initial polarization plane:

$$\alpha(\rho, \theta) = \tan^{-1} \left(\frac{E'_x}{E'_y} \right) = \tan^{-1} \left[\frac{\tan \xi(\rho) \sin 2\theta}{1 + \tan \xi(\rho) \cos 2\theta} \right]$$

$$\approx \xi(\rho) \sin 2\theta. \quad (7)$$

Here we took into account that components E'_x and E'_y are real.

The maximal rotation of the polarization plane is near the diagonal directions ($\theta = \pm 45$ deg) and equals about ξ . The direction of rotation is positive in the first and third quadrants and negative in the second and fourth quadrants. The exact value of the maximal rotation, α_{\max} , equals $\tan^{-1}[\tan \xi / (1 - \tan^2 \xi)^{1/2}]$ and is observed at $\theta_{\max} = \pm[45 \text{ deg} + (1/2)\alpha_{\max}]$. Hence, the distribution of the polarization plane rotation and the intensity distribution in the Maltese cross are not quite symmetrical to the diagonal axes.

In the case where there is only radial retardance, the field vector of an output ray is

$$\mathbf{E}' = e^{i\Delta_s} \begin{pmatrix} \cos \frac{\Delta}{2} + i \sin \frac{\Delta}{2} \cos 2\theta \\ i \sin \frac{\Delta}{2} \sin 2\theta \end{pmatrix}. \quad (8)$$

The output rays are elliptically polarized with azimuth γ and axes ratio σ :

$$\gamma = \frac{1}{2} \tan^{-1} \left[\frac{\tan^2(\Delta/2) \sin 4\theta}{1 + \tan^2(\Delta/2) \cos 4\theta} \right] \approx 0$$

and

$$\sigma = \frac{\sin \Delta \sin 2\theta}{1 + (1 - \sin^2 \Delta \sin^2 2\theta)^{1/2}} \approx (1/2) \sin \Delta \sin 2\theta. \quad (9)$$

Hence, the long axis of the vibration ellipse is almost parallel to the initial polarization plane. The ellipticity is maximal in the diagonal directions and is zero for $\theta = 0$ and 90 deg. The sign of the ellipses are opposite in neighboring quadrants.

Usually the entrance pupil of a microscope is illuminated with a uniform beam $I(\rho, \theta) = \text{const}$, and $\eta^{-1}(\rho) \ll 1$. So from Eq. (4), we obtain

$$\kappa = \frac{\pi}{\int_0^{2\pi} \int_0^1 \rho \{ \tan^2 \xi(\rho) + \sin^2[\Delta(\rho)/2] \} \sin^2 2\theta d\rho d\theta}$$

$$= \frac{1}{\int_0^1 \rho \{ \tan^2 \xi(\rho) + \sin^2[\Delta(\rho)/2] \} d\rho}. \quad (10)$$

When the initial beam has left circular polarization $\mathbf{E} = (1/\sqrt{2}) \begin{pmatrix} 1 \\ i \end{pmatrix}$, then the output polarization \mathbf{E}' is most conveniently described as a superposition of left and right circular polarization states \mathbf{E}'_l and \mathbf{E}'_r :

$$\mathbf{E}' = \mathbf{E}'_l + \mathbf{E}'_r = \frac{1}{2\sqrt{2}} T_s e^{i\Delta_s} (\mu e^{i\Delta} + 1) \begin{pmatrix} 1 \\ i \end{pmatrix}$$

$$+ \frac{1}{2\sqrt{2}} T_s e^{i\Delta_s} (\mu e^{i\Delta} - 1) e^{i2\theta} \begin{pmatrix} 1 \\ -i \end{pmatrix}. \quad (11)$$

The extinction η of a ray is determined by

$$\eta = \frac{E'_l(E'_l)^*}{E'_r(E'_r)^*} = \frac{(\mu+1)^2 - 4\mu \sin^2(\Delta/2)}{(\mu-1)^2 + 4\mu \sin^2(\Delta/2)}$$

$$\approx \frac{1}{\tan^2 \xi + \sin^2(\Delta/2)}. \quad (12)$$

Hence, in the case of crossed circular polarizers, the distribution of light in the exit pupil corresponds to a dark central area surrounded by a bright ring. Extinction factor κ of the complete optical system is determined by the ratio

$$\kappa = \frac{\pi}{\int_0^{2\pi} \int_0^1 \rho \{ \tan^2 \xi(\rho) + \sin^2[\Delta(\rho)/2] \} d\rho d\theta}$$

$$= \frac{1}{2 \int_0^1 \rho \{ \tan^2 \xi(\rho) + \sin^2[\Delta(\rho)/2] \} d\rho}. \quad (13)$$

When comparing Eqs. (10) and (13) we can see that the extinction factor for systems with crossed linear polarizers is twice as great than for crossed circular polarizers under otherwise the same conditions. Moreover, the extinction of a system with crossed circular polarizers can further deteriorate by the use of imperfect quarter-wave plates for the circular polarizers.

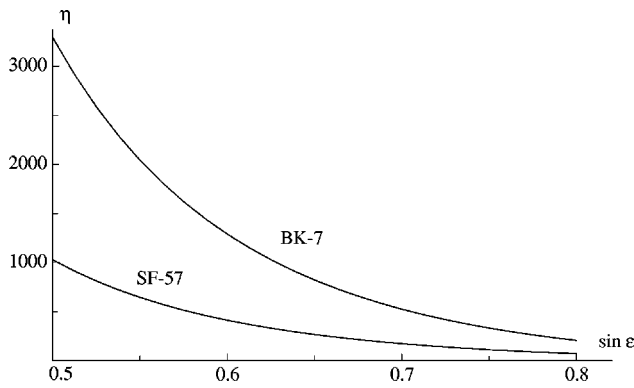


Fig. 1 Ray extinction η versus the sine of the incidence angle ϵ for single dry plane parallel plates made from Schott glasses BK-7 ($n = 1.51$) and SF-57 ($n = 1.84$).

3 Radially Symmetric Polarization Aberrations of Lenses and Plane Parallel Plates

3.1 Plane Parallel Plates

Glass plane parallel plates are often used between the condenser and objective lens of a microscope, for example, as the “slide” glass, cover slip, etc. Between the two, the specimen may be homogeneously immersed or mounted in media of various refractive indices. Usually the glass plates do not have any surface coatings. Let us consider the polarization aberrations contributed by a plate like this. Incidence and refractive angles are noted as ϵ and ϵ' , respectively. The refractive index of the plate is n . The focused beam has an NA. We note that the multiple beam interference inside the plate can ordinarily be neglected. We assume that there is no phase shift between the p - and s -polarization components (Sec. 1.2 in Ref. 14). As follows from the Fresnel formulas,¹⁴ the amplitude transmission ratio after passing the two surfaces of a dry plane parallel plate is

$$\mu = 1 + \tan^2(\epsilon - \epsilon'). \tag{14}$$

Taking into account that $\sin \epsilon_{\max} = \text{NA}$ and $\rho = 1$ for the marginal ray, we obtain

$$\sin \epsilon = \rho \text{NA} \quad \text{and} \quad \sin \epsilon' = \frac{\rho}{n} \text{NA}. \tag{15}$$

So the angle ξ can be found by

$$\tan \xi = \frac{n^2 - [\sin^2 \epsilon + \cos \epsilon (n^2 - \sin^2 \epsilon)^{1/2}]^2}{n^2 + [\sin^2 \epsilon + \cos \epsilon (n^2 - \sin^2 \epsilon)^{1/2}]^2}. \tag{16}$$

Figure 1 shows the dependence of the ray extinction η on the sine of the incidence angle ϵ for plates made from Schott glasses BK-7 ($n = 1.51$) and SF-57 ($n = 1.84$). The extinction applies for a circularly polarized ray or a linearly polarized ray with an azimuth of 45 deg. As we can see, the plate with higher refractive index glass introduces more polarization aberration. Theoretical studies of the rotation

of polarized light by plane parallel plates, based on similar principles and with experimental verification, were published by Wright¹⁵ in 1923.

3.2 Uncoated Lenses

Let us consider a thin positive lens without coating.¹² Curvature radii of the first and second surfaces are R_1 and R_2 . The focal length of the lens is f . Thus, the lens shape factor K is

$$K = (n - 1) \frac{f}{R_1}. \tag{17}$$

Incidence and refractive angles on the first and the second surfaces are noted as $\epsilon_1, \epsilon'_1, \epsilon_2,$ and ϵ'_2 , respectively.

The amplitude transmission ratio after passing the two lens surfaces is

$$\mu = \frac{1}{\cos(\epsilon_1 - \epsilon'_1) \cos(\epsilon_2 - \epsilon'_2)}. \tag{18}$$

As can be shown, a lens with equal differences $\epsilon_1 - \epsilon'_1$ and $\epsilon_2 - \epsilon'_2$ induces a minimal angle ξ and correspondingly minimal polarization aberrations. A similar method for minimizing depolarization in lenses was proposed by Wright¹⁵ in 1923.

In the case where a collimated axial beam falls on the lens

$$(\epsilon_1 - \epsilon'_1) - (\epsilon'_2 - \epsilon_2) = \Omega, \tag{19}$$

where Ω is the angle by which a ray is tilted to the lens axis after passing through the lens. Thus, for an optimal lens the incidence and refractive angles are $(\epsilon_1 - \epsilon'_1) = (\epsilon'_2 - \epsilon_2) = \Omega/2$ and $\eta = [1 + \cos^2(\Omega/2)]^2 / \sin^4(\Omega/2)$. For example, if $\sin \Omega = 0.3$, then $\eta \approx 7700$.

A plane convex lens with the plane as the first surface has the shape factor $K = 0$ and differences $\epsilon_1 - \epsilon'_1 = 0$ and $\epsilon'_2 - \epsilon_2 = \Omega$. Therefore its extinction is $\eta = 1 / [\tan^4(\Omega/2)]$. If $\sin \Omega = 0.3$, then $\eta \approx 1900$, that is, four times less than for the optimal lens.

Figure 2 gives the extinction as a function of the shape factor for lenses made from Schott glasses BK-7 ($n = 1.51$) and SF-57 ($n = 1.84$). This extinction corresponds to a circularly polarized ray or a linearly polarized ray with an azimuth of 45 deg. The initial ray is parallel to the lens axis. The ray angle Ω in the image field corresponds to $\text{NA} = 0.3$. A drawing of lenses that conforms to the shape factor K is shown below the graph.

As we can see the uncoated lenses from different refractive glasses have the same maximal extinction of about 7700, which drops to about 1900 when the first surface is plane. Hence, the beam depolarization depends on the lens shape factor. Lenses possessing shape factors between 0.5 and 1.0 have maximal extinction. Hence, lenses that produce about equal bending of the ray at both surfaces have the best extinction. It is interesting to note that those lenses also produce minimal spherical aberration. In contrast, menisci produce maximal polarization aberrations.

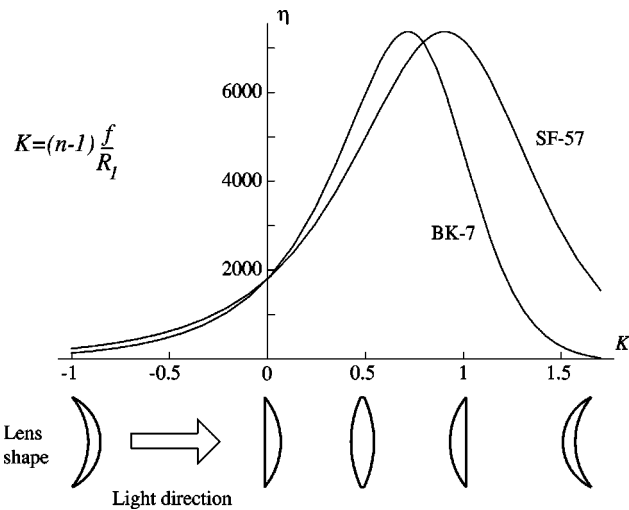


Fig. 2 Ray extinction η of a ray with NA=0.3 versus the shape factor K for single lenses made from Schott glasses BK-7 ($n = 1.51$) and SF-57 ($n = 1.84$). At the bottom of the figure, drawings of lenses are shown that correspond to the shape factors (light passes the lenses from left to right).

4 Measurement of Radially Symmetric Polarization Aberrations

4.1 Rotated Polarizer Technique

The first scheme for measuring the differential transmission and phase shift between the p - and s -polarization components is presented in Fig. 3. Here the optical system with radial polarization aberrations is placed between a linear polarizer and analyzer. One of them can be turned. A Bertrand lens creates an image of the exit pupil on a video camera. If the polarizer and analyzer are crossed, the image shows a cross shape (Maltese cross) [see Fig. 4(a)]. When the analyzer is turned by an angle χ from the crossed position, the intensity distribution $I(\rho, \theta)$ in the image is

$$I(\rho, \theta) = \left\{ [\sin(2\theta - \chi) \tan \xi(\rho) - \sin \chi]^2 + \sin^2(2\theta - \chi) \sin^2 \frac{\Delta(\rho)}{2} \right\} I', \quad (20)$$

where it is assumed that values ξ and Δ are small, and I' is the initial intensity distribution after the polarizer. Hence, the cross transforms into two arcs [see Fig. 4(b)]. The distance between the arcs depends on the analyzer azimuth and the values of differential transmission. It can be shown that if radial retardance is nonzero and overwhelms the differential transmission, then rotating the analyzer will not produce dark arcs but will cause the cross to fade away.

For a point A at radius ρ along the diagonal with azimuth coordinate $\theta = 45$ deg the intensity is

$$I_A = \left\{ [\tan \xi(\rho) - \sin \chi]^2 + \sin^2 \frac{\Delta(\rho)}{2} \right\} I'. \quad (21)$$

In this equation, we assume that χ is small and neglect terms with χ^4 and more.

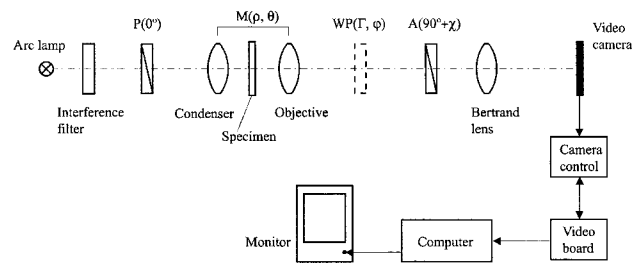


Fig. 3 Optical setup for measuring differential transmissions and phase shifts: $M(\rho, \theta)$, microscope optical system under investigation; $P(0$ deg), polarizer with an azimuth of 0 deg; $A(90$ deg + $\chi)$, analyzer with an azimuth of 90 deg + χ ; $WP(\Gamma, \varphi)$; compensation wave plate with small retardance Γ and an azimuth of φ .

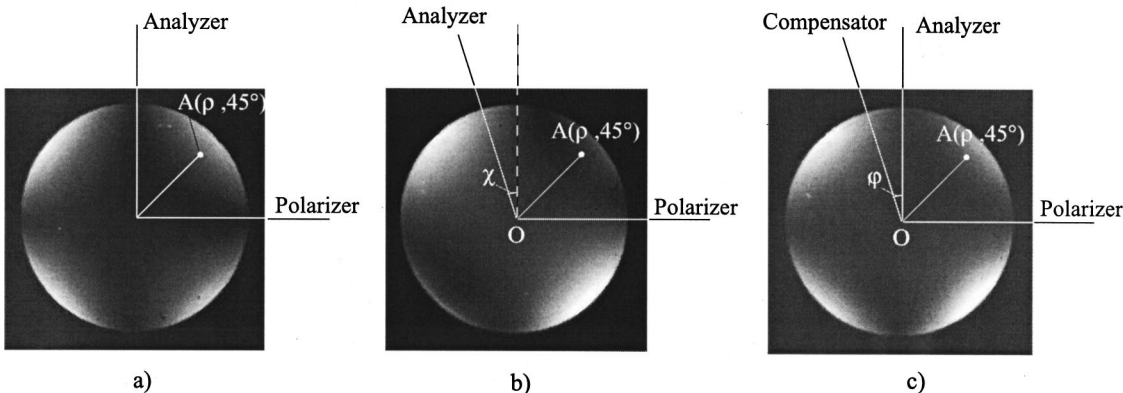


Fig. 4 Images of the back aperture of a microscope objective between linear polarizer and analyzer during measurements of differential transmission and phase shift between the p - and s -polarization components: (a) polarizer and analyzer crossed, (b) analyzer rotated by a small angle, and (c) polarizer and analyzer crossed and compensation wave plate rotated by a small angle.

The intensity at a point A along the diagonal is a minimum \tilde{I}_A when $\chi = \xi(\rho)$:

$$\tilde{I}_A = I' \sin^2 \frac{\Delta(\rho)}{2}. \quad (22)$$

The polarization turn angle ξ and retardance Δ are equal to zero at the center point $O(\rho=0)$. The center point intensity I_O is

$$I_O = I' \sin^2 \chi = I' \tan^2 \xi(\rho). \quad (23)$$

Thus, we can find the angle $\xi(\rho)$ by rotating one of the polarizers to find the minimum intensity at a point A with radius ρ and azimuth $\theta = 45^\circ$. At minimum intensity we have

$$\xi(\rho) = \chi. \quad (24)$$

If the minimum intensity is not zero, the lens also possesses radial retardance. To determine the radial retardance we measure the minimum intensity \tilde{I}_A at the point A and the intensity \tilde{I}_O in the center of the pattern. Then the radial retardance $\Delta(\rho)$ is

$$\begin{aligned} |\Delta(\rho)| &= 2 \sin^{-1} \left[\left(\frac{\tilde{I}_A}{\tilde{I}_O} \right)^{1/2} \tan \chi \right] \\ &\approx 2\chi \left(\frac{\tilde{I}_A}{\tilde{I}_O} \right)^{1/2} = 2\xi(\rho) \left(\frac{\tilde{I}_A}{\tilde{I}_O} \right)^{1/2}. \end{aligned} \quad (25)$$

This technique does not enable us to distinguish the slow and fast axes of the lens retardance. Also, the measurement requires a flat intensity distribution in the entrance pupil plane or Eq. (25) should be corrected.

4.2 Rotated Compensator Technique

It is also possible to employ a rotating compensator made of a wave plate with retardance Γ below 20 deg to find the radial differential transmittance and retardance of a lens. The compensator is shown in Fig. 3 by dashed lines. The polarizer and analyzer are crossed. In case of small values ξ and Δ , the intensity distribution $I(\rho, \theta)$ in the image of the exit pupil is described by

$$\begin{aligned} I(\rho, \varphi) &= \left\{ \sin^2 2\theta \tan^2 \xi(\rho) \right. \\ &\quad \left. + \left[\sin \frac{\Gamma}{2} \sin 2\varphi + \sin \frac{\Delta(\rho)}{2} \sin 2\theta \right]^2 \right\} I', \end{aligned} \quad (26)$$

where φ is the azimuth of the slow axis of the compensator, and I' is the initial distribution of intensity after the polarizer.

When $\varphi = 0$ deg [see Eq. (26)], the intensity is $I(\rho, \theta) = 0$ for points with $\theta = 0$ deg and $\theta = 90$ deg. This results in a cross at the back aperture similar in appearance to the cross generated by differential transmission alone. How-

ever, if the compensator is turned by an angle $\varphi \neq 0$, then the cross transforms into two arcs. The distance between the arcs depends on the compensator azimuth and the value of radial retardance. In the presence of differential transmission that overwhelms the radial retardance, the cross fades away when the compensator is rotated.

For the diagonal point A with azimuth coordinate $\theta = 45$ deg the intensity is

$$I_A = \left\{ \tan^2 \xi(\rho) + \left[\sin \frac{\Gamma}{2} \sin 2\varphi + \sin \frac{\Delta(\rho)}{2} \right]^2 \right\} I'. \quad (27)$$

This intensity has a minimum \tilde{I}_A when $\sin(\Gamma/2)\sin 2\varphi = -\sin[\Delta(\rho)/2]$. Hence,

$$\Delta(\rho) = -\Gamma \sin 2\varphi, \quad \text{and}$$

$$\tilde{I}_A = I' \tan^2 \xi(\rho). \quad (28)$$

Simultaneously the center point intensity I_O is

$$I_O = I' \sin^2 \frac{\Gamma}{2} \sin^2 2\varphi = I' \sin^2 \frac{\Delta(\rho)}{2}. \quad (29)$$

Thus, we can find the radial retardance $\Delta(\rho)$ by searching for the minimum intensity in a point A with radius ρ and $\theta = 45$ deg and then determine the angle $\xi(\rho)$ by measuring the intensities \tilde{I}_A and the center point intensity \tilde{I}_O when the minimum has been found:

$$\begin{aligned} \xi(\rho) &= \tan^{-1} \left[\left(\frac{\tilde{I}_A}{\tilde{I}_O} \right)^{1/2} \sin \frac{\Gamma}{2} \sin 2\varphi \right] \\ &\approx \frac{1}{2} \Gamma \sin 2\varphi \left(\frac{\tilde{I}_A}{\tilde{I}_O} \right)^{1/2} = -\frac{\Delta(\rho)}{2} \left(\frac{\tilde{I}_A}{\tilde{I}_O} \right)^{1/2}. \end{aligned} \quad (30)$$

This second technique with a rotating compensator enables us to determine the sign of the lens retardance, but it precludes us from finding the sign of the angle $\xi(\rho)$. On the other hand, the first technique with the rotating analyzer enables us to determine the sign of the angle $\xi(\rho)$ but does not give us the possibility to find the sign of the lens retardance.

The described experimental procedures measure polarization aberrations of the complete microscope optical system. Other techniques could be employed to measure the 2-D distribution of retardance and differential transmission, for example, by Mueller matrix imaging polarimetry,¹⁶ polarized light microscopy using the universal liquid crystal compensator,¹⁷ or phase shifting techniques.^{18,19} If it is necessary to find aberrations introduced by a single optical component such as the objective or condenser lens separately, the polarization aberrations of the other components in the system should be known beforehand. Otherwise, one can either use a pair of identical lenses as condenser and objective²⁰ or use a return path technique²¹ to measure the differential transmittance and radial retardance of either a single objective or a condenser.

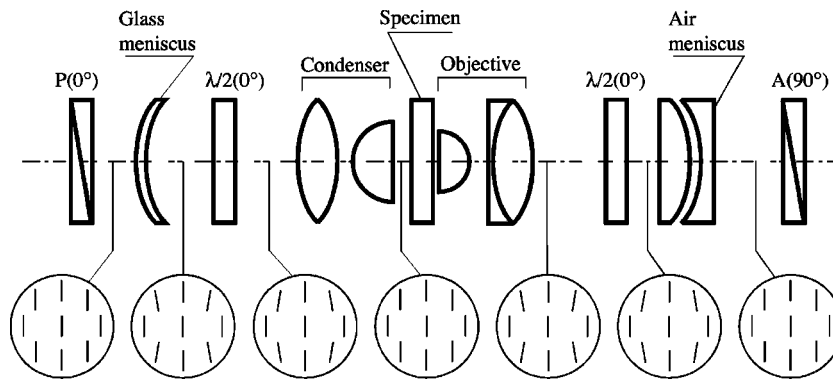


Fig. 5 Meniscus rectifier for linearly polarized beam (Ref. 20).

In Sec. 6 we present measurements of polarization aberrations of high-NA microscope lenses using the experimental procedures just described. However, first we discuss ways to reduce or almost eliminate polarization aberrations in high-NA imaging systems.

5 Rectification of Depolarization in a High-NA Microscope

To reduce the beam depolarization in a high-NA microscope a polarization rectifier can be used.²⁰ Here two kinds of rectifiers are described. The first contains a zero-power meniscus. The second kind uses a sectored liquid crystal compensator. We can put one rectifier in the illumination path of the microscope before the condenser lens, or in the imaging path after the objective lens or two rectifiers in both places. In the last case different condenser and objective lenses can be combined in the microscope and in addition, a more uniform polarization pattern is produced in the specimen plane.

The first scheme of polarization rectifier^{20,22} with a meniscus is shown in Fig. 5. It can be used to decrease the depolarization of a linearly polarized beam. The rectifier consists of a glass or air meniscus with zero optical power and a half-wave plate. The meniscus creates the same distribution of the polarization rotation angle and ellipticity as the compensated optical element. The principal axis of the half-wave plate is parallel to the polarizer P. The half-wave plate flips the rotated polarization with respect to the plate's principal axis and then the condenser or the objective or both compensate this rotation. Thus, in the exit pupil, the beam has the correct linear polarization distribution and will be extinct by the analyzer A. In the optical schematic of Fig. 5, the different distributions of beam polarizations between elements of the microscope are illustrated. The differential transmission of lenses rotates the polarization plane of rays in the direction of the plane of incidence (the radial direction), as shown in the diagrams. The rotation is zero if the electric vector is parallel or perpendicular to the plane of incidence and maximum for $\theta \approx 45$ deg.

The first scheme of meniscus rectifier is described by the matrix equation

$$\mathbf{E}' = \mathbf{M}_{\text{micr}} \cdot \mathbf{M}_{\lambda/2}(0 \text{ deg}) \cdot \mathbf{M}_{\text{rect}} \cdot \mathbf{E}, \quad (31)$$

where \mathbf{E}' and $\mathbf{E} = \begin{pmatrix} 1 \\ 0 \end{pmatrix}$ are the field vectors of the output and input beams, \mathbf{M}_{micr} is the Jones matrix of the microscope optical system, $\mathbf{M}_{\lambda/2}(0 \text{ deg})$ is the matrix of the half-wave plate with an azimuth of 0 deg and \mathbf{M}_{rect} is the matrix of the meniscus rectifier. Taking into account that the matrices of the optical system and rectifier are the same [see Eq. (1)] and $\mathbf{M}_{\lambda/2}(0 \text{ deg}) = \begin{pmatrix} 1 & 0 \\ 0 & -1 \end{pmatrix}$ we obtain

$$\mathbf{E}' = \frac{1}{4} T_s^2 \times \begin{bmatrix} (\mu e^{i\Delta} + 1)^2 + 2(\mu^2 e^{i2\Delta} - 1) \cos 2\theta + (\mu e^{i\Delta} - 1)^2 \cos 4\theta \\ (\mu e^{i\Delta} - 1)^2 \sin 4\theta \end{bmatrix}. \quad (32)$$

So this rectifier does not remove the orthogonal component completely. The extinction ratio η of a ray is

$$\eta \approx \frac{1}{[\tan^2 \xi + \sin^2(\Delta/2)]^2 \sin^2 4\theta}. \quad (33)$$

If $\tan \xi = \sin(\Delta/2) = 0.05$, then the extinction ratio is improved 100 times compared to the case without the rectifier [see Eq. (5)]. Figure 6 shows pupil images recorded with a microscope equipped with such meniscus rectifiers.

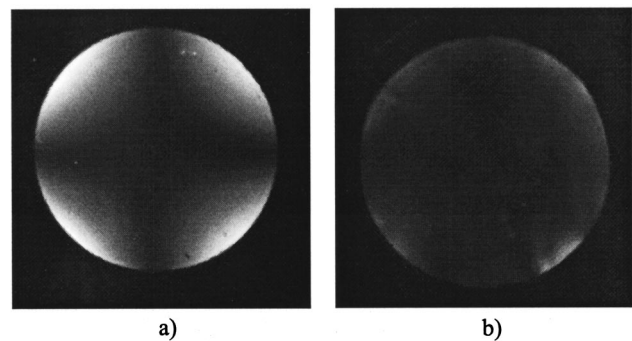


Fig. 6 Images of the back aperture of a pair 1.25-NA oil immersion objectives Spencer 97× (American Optical Corporation) with single-layer MgF₂ antireflection coatings between crossed polarizers (a) without rectifiers and (b) equipped with meniscus rectifiers. Exposure time in the second case is increased 10 times.

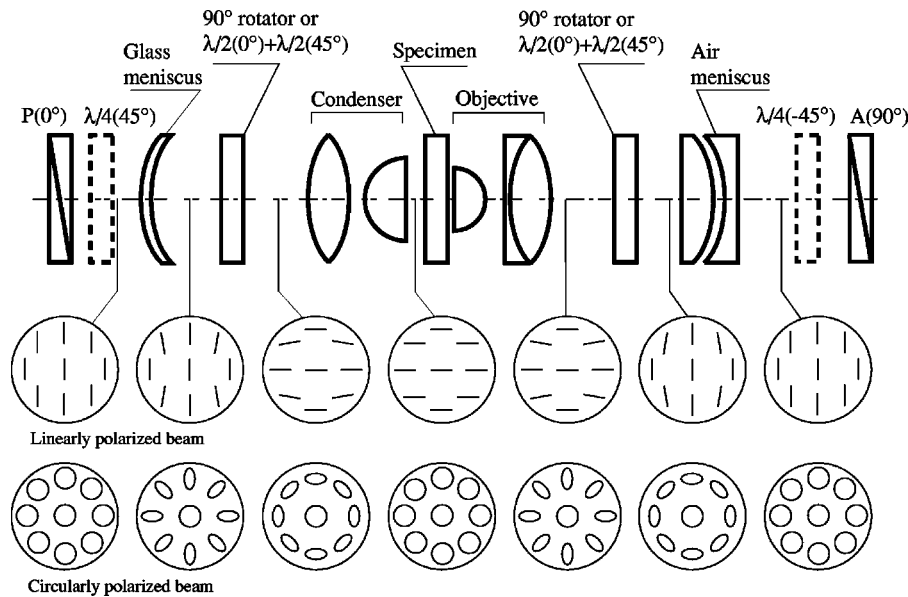


Fig. 7 Optical system with universal meniscus rectifier.

For circularly polarized light, the first rectifier scheme was improved by the addition of a second half-wave plate that is turned by 45 deg with respect to the first half-wave plate.²³ This combination of half-wave plates can be replaced by a 90-deg polarization rotator made from an optically active crystal, which is cut perpendicular to its optic axis. For example, a z-cut quartz plate with thickness 3.8 mm can be used as a 90-deg rotator for $\lambda = 546$ nm. In addition, optical coatings that are applied to the meniscus and introduce the same radial retardance as the microscope optical system can compensate the influence of the microscope radial retardance. We call the meniscus with a 90-deg rotator a universal meniscus rectifier (see Fig. 7). Shortly we show that the universal meniscus rectifier enables rectification of a beam with any initial polarization state. Figure 7 shows the different distributions of beam polarizations for a linearly and circularly polarized beam. In the latter case using a circularly polarized beam, the differential transmission of lenses squeezes the polarization ellipse of rays in the tangential direction, as shown in the diagrams.

The universal meniscus rectifier is described by the following matrix equation:

$$\mathbf{E}' = \mathbf{M}_{\text{micr}} \cdot \mathbf{M}_{\text{rot}}(90 \text{ deg}) \cdot \mathbf{M}_{\text{rect}} \cdot \mathbf{E}, \quad (34)$$

where \mathbf{E}' and \mathbf{E} are the field vectors of the output and input rays, \mathbf{M}_{micr} is the Jones matrix of the microscope optical system, $\mathbf{M}_{\text{rot}}(90 \text{ deg})$ is the matrix of the 90-deg rotator, and \mathbf{M}_{rect} is the matrix of the meniscus rectifier. Here the matrices of the optical system and rectifier are equal and include the differential transmittance and radial retardance terms [see Eq. (1)] and $\mathbf{M}_{\text{rot}}(90 \text{ deg}) = \begin{pmatrix} 0 & 1 \\ -1 & 0 \end{pmatrix}$. After forming the matrix product of the matrices, we find the Jones matrix of the microscope with rectifier:

$$\begin{aligned} & \mathbf{M}_{\text{micr}} \cdot \mathbf{M}_{\text{rot}}(90 \text{ deg}) \cdot \mathbf{M}_{\text{rect}} \\ & = T_p T_s \exp[i(\Delta_p + \Delta_s)] \begin{pmatrix} 0 & 1 \\ -1 & 0 \end{pmatrix}. \end{aligned} \quad (35)$$

As follows from the obtained matrix, the microscope will preserve the polarization structure of the entrance pupil. This enables us to completely remove the depolarization caused by differential transmission and radial retardance for any initial polarization state. The electric field vectors of the output rays will be turned by 90 deg compared to the initial polarization.

An alternative design for a rectifier uses sectored liquid crystal compensators for correcting a beam with arbitrary polarization distribution (see Fig. 8). It consists of two sectored liquid crystal cells LCA and LCB. Both cells are divided into one central circular sector and eight side sectors as shown in the lower diagrams of Fig. 8. The slow axes of the sectors in a cell have the same orientation. The slow axis of the first cell LCA is turned by 45 deg with respect to the polarizer P.

The second cell LCB has the slow axis oriented parallel to the polarizer P. The retardance magnitude of each sector can be set independently of all the other sectors. Hence, each sector in the polarizer-LCA-LCB assembly functions as a universal compensator, as described earlier by Oldenbourg and Mei.¹⁷ Diagrams under the optical schematic in Fig. 8 illustrate the polarization states of an initially linearly and circularly polarized beam when the radial differential transmittance is the dominant source of depolarization. When the optical system has additional radial retardance, the sectored compensator can also improve the extinction, but the detailed description of its effect becomes more complicated.

In the case of linear polarization, the compensator works in the following manner. The linearly polarized beam

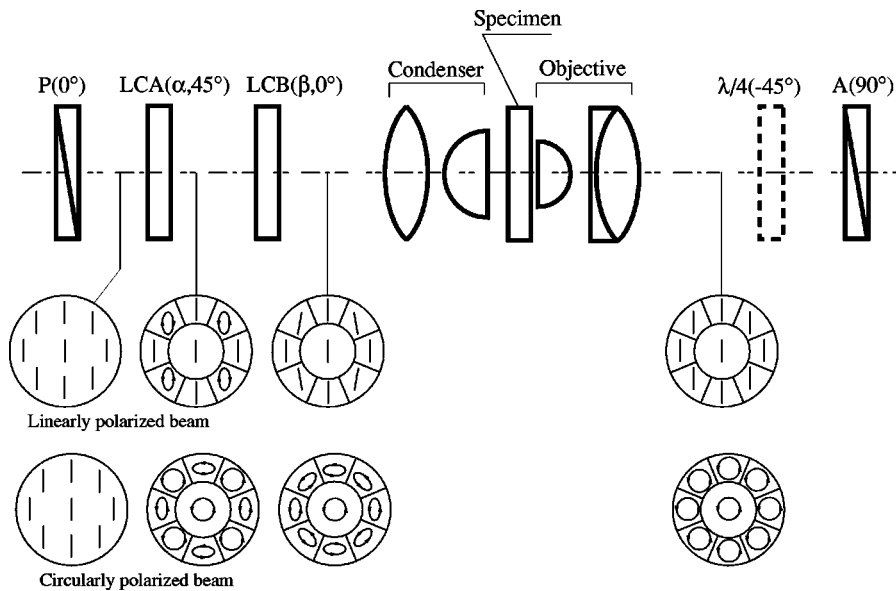


Fig. 8 Optical system with liquid crystal sectored rectifier.

passes through the first cell LCA and then the second cell LCB. The retardance values of the central sector and the horizontal and vertical side sectors are adjusted so as to not change the polarization state of the beam. These sectors have zero retardance for cell LCA and any retardance for cell LCB. The diagonal sectors rotate the beam polarization as it is shown in the diagram (middle row, Fig. 8). The magnitude of this rotation is chosen so as to obtain maximal extinction for each diagonal sector and is about 0.9ξ . Here ξ is the amount of rotation of the polarization plane of the marginal ray at the edge of the aperture and an azimuth of 45 deg. Thus retardance values of the diagonal sectors are $\pm 1.8\xi$ for cell LCA and 90 deg for cell LCB. As one can see, for linearly polarized light, the second cell can be replaced by a quarter-wave plate.

For rectification of circularly polarized light, it is necessary to have a circularly polarized beam after the central sectors and elliptically polarized side beams (bottom diagram, Fig. 8). The axes ratio of the polarization ellipses is $\tan[45 \text{ deg} - (\xi/2)]$. This ratio is used to maximize the extinction for each side sector. In cell LCA the central and diagonal sectors have 90-deg retardance, the horizontal sectors have $90 \text{ deg} - \xi$ retardance and the vertical sectors have $90 \text{ deg} + \xi$ retardance. The central sector and horizontal and vertical side sectors of cell LCB do not change the polarization state of the beam and have zero retardance. The diagonal sectors of cell LCB have retardance $90 \text{ deg} \pm \xi$. Hence, the vibration ellipses of side beams have the small axis in the radial direction. The radial differential transmittance of the optical system squeezes the ellipses in the tangential direction and almost circularly polarized side beams fall on the circular polarizer that consists of a quarter-wave plate $\lambda/4(-45 \text{ deg})$ and a linear polarizer A(90 deg). Figure 9 shows images of the sectored liquid crystal rectifier built into the front focal plane of the condenser lens of a microscope.

6 Experimental Results

Using techniques described in Sec. 5 we measured the distribution of differential transmission and phase shift in several microscope objective and condenser lenses. Our experimental setup was based on a Nikon Microphot SA microscope equipped with a Brace-Köhler compensator with 23-deg retardance at a wavelength of 546 nm and a bandpass filter (made by Chroma Technology Corp. in Brattleboro, Vt.) with a central wavelength of 546 nm and 12-nm FWHM. For image capture, a Dage-MTI C300 video camera was used. We measured aberrations in the lens combination of an oil immersion objective CFN DIC Plan Apochromat $60\times/1.4 \text{ NA}$ (Nikon, part 85033) and Nikon Achromat-Aplanat condenser lens with an aperture of 1.4, and the combination of a dry objective CFN DIC Plan Achromat $40\times/0.7 \text{ NA}$ (Nikon, part 85031) and the same

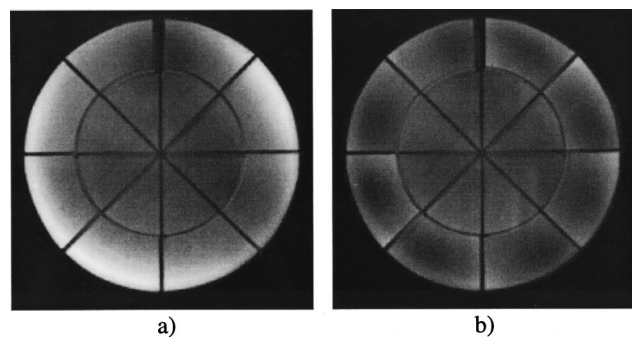


Fig. 9 Images of the liquid crystal sectored rectifier that is placed in the front focal plane of the 0.9-NA condenser lens in a Zeiss microscope Axiovert 200M equipped with a dry antireflective coated objective Plan-NEOFLUAR $40\times/0.85\text{Po}1$ and left circular analyzer: (a) sectors that are part of one cell have same retardance values and (b) each sector has individually adjusted retardance values for maximum extinction.

Table 1 Calculated (η_{calc}) and measured (η_{exp}) extinction, maximum turn angle (ξ_{max}), and retardance (Δ_{max}) measured in the pupil plane of microscope lenses made by American Optical Corporation (United States) and Nikon (Japan). NA is the numerical aperture of the objective and condenser lenses. The ratio $\eta_{\text{exp}}/\eta_{\text{calc}}$ is also given.

Objective	NA	ξ_{max} (deg)	Δ_{max} (deg)	η_{calc}	η_{exp}	$\eta_{\text{exp}}/\eta_{\text{calc}}$
AO Spencer 97 \times , SFC	1.25 (oil)	5.5	2.0	600	600	1.0
AO Spencer 97 \times , SFR (with rectifier)	1.25 (oil)	0.5	2.5	8800	5100	0.58
Nikon Plane 40 \times	0.7	8.0	2.5	670	600	0.90
Nikon PlanApo 60 \times	1.40 (oil)	5.5	6.0	450	430	0.96

condenser used without oil immersion. Both objectives and condenser were designated for differential interference contrast (DIC) microscopy and are of good polarization quality. The Nikon objectives and condenser have multilayer antireflection coatings. In both cases, a test sample with diatoms (made by Carolina Optical Supply Co.) was placed between objective and condenser lenses. Also we studied two pairs of oil immersion, strain-free objectives, Spencer 97 \times with NA=1.25 (made by Optical Corporation of America around 1957). One objective pair included meniscus rectifiers for linearly polarized light. The Spencer objectives are coated by a single-layer antireflection coating of MgF₂. These objectives were first analyzed by Inoué and Hyde²⁰ in 1957, who first indicated that antireflection coatings and immersion liquids can reduce polarization aberrations in microscopes. Thus, it is possible to compare our results with those obtained over 40 years ago. For image processing and data analysis, we used NIH Image (public domain software, available at <http://rsb.info.nih.gov/nih-image/>) and Mathematica (Wolfram Research, Champaign, Illinois).

For each combination of objective and condenser lenses, we measured in the exit pupil the intensity along a line through the pupil center and oriented at 45 deg (see Fig. 4). Several such intensity profiles that were measured for different polarizer and compensator settings were combined to yield the turn angle $\xi(\rho)$, which describes differential transmission, and retardance $\Delta(\rho)$, which describes differential phase shift, each as a function of radial position in the pupil. Based on the pupil function measurements we calculated a theoretically predicted extinction factor in the image plane, using Eq. (10). Note that the formulas were obtained assuming a uniform intensity distribution in the pupil plane. But the formulas can easily be corrected for other kinds of radially symmetric intensity distributions, according to Eq. (3), for instance, a Gaussian distribution.

As mentioned in Sec. 2, there are other sources of depolarization in optical system. Therefore, we determined the extinction factor experimentally by measuring intensities of light in the image plane with parallel and crossed polarizer and analyzer. The ratio between the theoretically calculated extinction factor and the experimental one shows the contribution of radially symmetric polarization aberration at total extinction. A more detailed description of the calculation procedure and additional experimental results will be published elsewhere.

Table 1 shows results for microscope lenses made by American Optical Corporation (United States) and Nikon (Japan). It can be seen that high-NA microscope objectives with antireflection coatings have large values of differential transmission and phase shift. The radially symmetric polarization aberrations contribute the dominant part in the total extinction in systems without polarization rectification. Differential transmission is significantly more for a dry system than for an immersion system. The meniscus rectifier reduced the radial differential transmission of the optical system but not its retardance, possibly because the meniscus has no dielectric coating applied. To decrease the radial retardance it is necessary to cover the meniscus by an antireflection coating with the same retardance as the compensated objective. The rectifier enables us to improve the extinction factor by about a factor of 10. Early measurements by Inoué and Hyde²⁰ using the same objective lenses and a restricted field size showed that the rectifier improved the extinction by a factor of more than 20 (extinction 13,000 compared to 600). The reduced extinction measured now might be caused by additional defects in the objective that have since then developed.

Our findings indicate that the measured value of extinction in the image plane does not depend on the distance from the measured point to the optical axes of the microscope. In other words, the measured extinction is uniform over the field of view. This observation confirms that the theory that is strictly correct for a point on the optical axis also applies to the available image plane.

Examples of the measured turn angle ξ and retardance Δ distribution as functions of the normalized pupil coordinate ρ are shown in Fig. 10. Here measurement results for two pairs of oil immersion, strain-free objectives Spencer 97 \times with NA=1.25 are presented. Both objectives are coated by a single-layer MgF₂ antireflection coating. As we can see, both turn angle and retardance dependence have almost radial symmetry and rise from a 0 value in the center of the pupil to a maximum measured at the pupil edge. We observed with all objectives that the radial symmetry of the turn angle distribution is more pronounced than the radial symmetry of the retardance distribution. This difference is probably due to a higher susceptibility of the retardance field to inner stress in lenses and other depolarization factors. Furthermore, the radial retardance distribution of the oil immersion objective Nikon PlanApo-60 \times shows a change of the retardance sign with radial coordinate. The

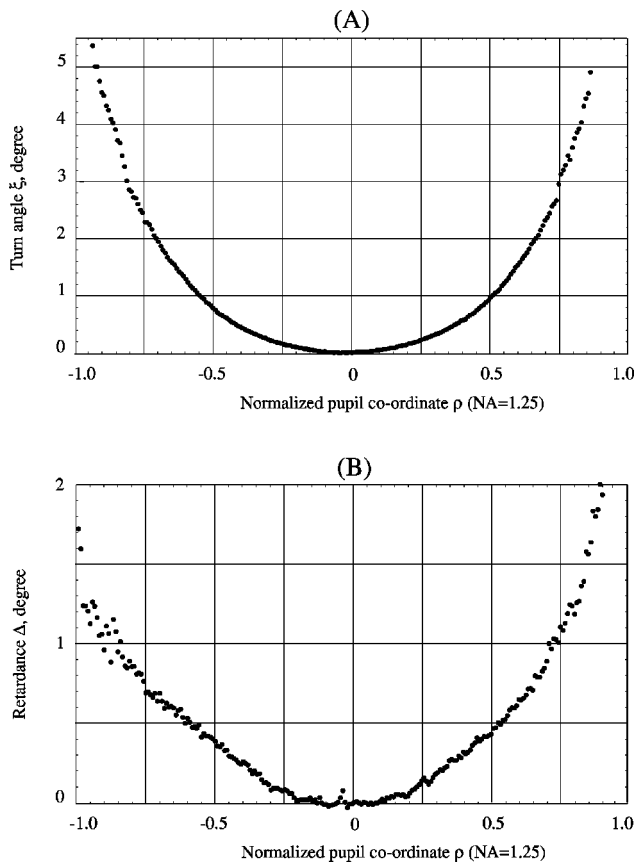


Fig. 10 Turn angle ξ (a) and retardance Δ (b) as a function of normalized pupil coordinate ρ of a pair of 1.25-NA oil immersion objectives Spencer 97 \times (American Optical Corporation) with single-layer MgF_2 antireflection coatings without rectifiers.

retardance is 0 for the axial point and for points that correspond to rays with NAs of about 0.7. It seems possible that in the case of complex multilayer antireflection coatings, the retardance sign of optical surface members δ_k in the summary retardance Δ [see Eqs. (2)] can be positive or negative dependent on the angle of incidence of rays that pass through the dielectric layers. Hence, the summary retardance can be compensated at some radii. Perhaps the members $\hat{\xi}_k$ in summary turn angle ξ have only one sign because $T_p > T_s$ and cannot compensate each other.

7 Conclusions

The radially symmetric polarization aberration introduced by lenses and plane parallel plates reduces the extinction and can lead to anomalous diffraction and modifies the point spread function. The extinction factor for systems with crossed linear polarizers is twice as great as that for crossed circular polarizers under otherwise the same conditions.

The extinction as a function of the NA for uncoated lenses and for plane parallel plates was calculated. Moreover, the connection between the shape factor of a lens and the extinction was determined. It was shown that a plate made from higher refractive glass introduces more depolarization than if it is made from lower refractive glass. The maximal extinction value of an uncoated lens with optimal

shape, however, does not depend on the refractive index. Lenses that possess shape factors between 0.5 and 1.0 give maximal extinction. Menisci produce strong depolarization.

Techniques for measuring differential transmission and radial retardance using a rotatable analyzer or compensator were described. The results of the measurement can be used to choose the optimal design of polarization rectifiers.

The function of polarization rectifiers with a meniscus and a sectored liquid crystal compensator were analyzed. The meniscus rectifier consists of a glass or air meniscus with zero-order optical power and a half-wave plate and was employed to decrease the depolarization of a linearly polarized beam as well as attendant anomalous diffraction.

The introduction of a 90-deg rotator instead of the half-wave plate made it possible to remove polarization aberrations for any initial polarization state. Furthermore, a sectored liquid crystal compensator can create a corrected beam with arbitrary polarization aberration.

Finally, experimental results on polarization aberrations measured in a rectified and a nonrectified microscope system were presented. Good agreement between experiment and theory was found.

Acknowledgment

This research was funded by the National Institutes of Health Grant No. GM49210 awarded to R.O.

References

1. F. E. Wright, *The Methods of Petrographic-Microscopic Research, Their Relative Accuracy and Range of Application*, Carnegie Institution of Washington, Washington, DC (1911).
2. S. Inoué and R. Oldenbourg, "Microscopes," Chap. 17 in *Handbook of Optics*, Vol. II, 2nd ed., M. Bass, Ed., pp. 17.1–17.52, McGraw-Hill, New York (1995).
3. S. Inoué and K. Spring, *Video Microscopy: The Fundamentals*, 2nd ed., pp. 76–86, Plenum Press, New York (1997).
4. R. A. Chipman and L. J. Chipman, "Polarization aberration diagrams," *Opt. Eng.* **28**(2), 100–106 (1989).
5. R. A. Chipman, "Polarimetry," Chap. 22 in *Handbook of Optics*, Vol. II, 2nd ed., M. Bass, Ed., pp. 22.1–22.37, McGraw-Hill, New York (1995).
6. S. Inoué and H. Kubota, "Diffraction anomaly in polarizing microscopes," *Nature (London)* **182**, 1725–1726 (1958).
7. H. Kubota and S. Inoué, "Diffraction images in the polarizing microscope," *J. Opt. Soc. Am.* **49**, 191–198 (1959).
8. J. P. McGuire and R. A. Chipman, "Diffraction image formation in optical systems with polarization aberration. I: Formulation and example," *J. Opt. Soc. Am. A* **7**(9), 1614–1626 (1990).
9. J. P. McGuire and R. A. Chipman, "Polarization aberration. 1. Rotationally symmetric optical systems," *Appl. Opt.* **33**(22), 5080–5100 (1994).
10. J. B. Uri, "Polarizations and interference in optics V. Lenses, imaging properties of lenses," *Optik (Stuttgart)* **49**, 375–378 (1978).
11. P. I. Lamekin and K. G. Predko, "Change of the polarization structure of axial polarized light beams by lens systems," *Opt. Spectrosc.* **60**, 137–142 (1986).
12. Y. M. Klimkov, M. I. Shribak, "Influence of lens shape on polarization modification of axial beam," *Izv. Vyssh. Uchebn. Zaved. USSR. Geodez. Aerophot.* **5**, 128–139 (1990).
13. T. Wilson and R. Juskaits, "On the extinction coefficient in confocal polarization microscopy," *J. Microsc.* **179**(3), 238–240 (1995).
14. M. Born and E. Wolf, *Principles of Optics*, 6th ed., pp. 38–47, Pergamon Press, Oxford (1987).
15. F. E. Wright, "The formation of interference figures a study of the phenomena exhibited by transparent inactive crystal plates in coherent polarized light," *J. Opt. Soc. Am.* **7**, 778–817 (1923).
16. J. L. Pezzanitti and R. A. Chipman, "Mueller matrix imaging polarimetry," *Opt. Eng.* **34**(6), 1558–1568 (1995).
17. R. Oldenbourg and G. Mei, "New polarized light microscope with precision universal compensator," *J. Microsc.* **180**(2), 140–147 (1995).
18. Y. Otani, T. Shimada, T. Yoshizawa, and N. Umeda, "Two-dimensional birefringence measurement using the phase shifting technique," *Opt. Eng.* **33**(5), 1604–1609 (1994).
19. Y. Otani, T. Shimada, and T. Yoshizawa, "The local-sampling phase

- shifting technique for precise two-dimensional birefringence measurement," *Opt. Rev.* **1**(1), 103–106 (1994).
20. S. Inoué and W. L. Hyde, "Studies on depolarization of light at microscope lens surfaces. II. The simultaneous realization of high resolution and high sensitivity with the polarizing microscopy," *J. Biophys. Biochem. Cytol.* **3**, 831–838 (1957).
 21. M. I. Shribak, Y. Otani, and T. Yoshizawa, "Return-path polarimeter for two dimensional birefringence distribution measurement," *Proc. SPIE* **3754**, 144–149 (1999).
 22. W. L. Hyde and S. Inoué, "Polarizing optical systems," U.S. Patent No. 2,936,673 (filed January 24, 1956).
 23. R. Oldenbourg and G. Mei, "Polarized light microscopy," U.S. Patent No. 5,521,705 (filed May 12, 1994).



Michael Shribak received his MSc in physical optics in 1982 from the Lviv State University, Ukraine, and his PhD in optics in 1991 from the Moscow University of Geodesy and Cartography, Russia. From 1982 to 1993 he was a senior scientist with the Electronic Research Institute, Lviv, Ukraine, from 1993 until 2000 he was a senior scientist with the Heat & Mass Transfer Institute, Minsk, Belarus, and from 1995 until 1998 he also held an appointment with LEMT (Lasers in Ecology, Medicine and Technology), Minsk, Belarus. In 1998 and 1999 he was a visiting professor with the Tokyo Agriculture and Technology University, Japan. In 2000 he became a staff scientist with Marine Biological Laboratory. He is the author of more than 90 scientific publications, among them 43 patents. His major research interests include the development of polarization imaging techniques for measuring birefringence distributions in two and three dimensions, fiber optical sensors, optical systems using laser diodes, and optical disk storage systems.



Shinya Inoué is a distinguished scientist with the Marine Biological Laboratory and a member of the National Academy of Sciences. He has contributed to advances in microscopy since the late 1940s. In addition to his path-breaking studies in cell biology, he invented the polarization rectifier and the centrifuge polarizing microscope, and pioneered in video microscopy. He is author of the book *Video Microscopy*, which is in its second edition and which has been translated into Spanish and Japanese.



Rudolf Oldenbourg received his Diplom (MS) in physics in 1976 from the Technical University in Munich, Germany, and his PhD in physics in 1981 from the University in Konstanz, Germany. He was a postdoctoral fellow from 1981 to 1983 at the University of Konstanz and in 1984 at Brandeis University in Waltham, Massachusetts. In 1984 he joined the physics faculty at Brandeis University and in 1989 became a faculty member of the Marine Biological Laboratory where he still is today. His research interests include polarized light microscopy, optical methods for imaging and manipulating living cells, the biophysics of cell motility, and cell biology.